HHS Public Access

Author manuscript

J Invest Dermatol. Author manuscript; available in PMC 2018 May 01.

Published in final edited form as:

J Invest Dermatol. 2017 May ; 137(5): 1015–1024. doi:10.1016/j.jid.2017.01.012.

Msi2 maintains quiescent state of hair follicle stem cells by directly repressing the Hh signaling pathway

Xianghui Ma[1,¶], **Yuhua Tian**[1,¶], **Yongli Song**[1], **Jianyun Shi**[1], **Jiuzhi Xu**[1], **Kai Xiong**[2], **Jia Li**[1], **Wenjie Xu**[1], **Yiqiang Zhao**[1], **Jianwei Shuai**[3], **Lei Chen**[4], **Maksim V. Plikus**[5], **Christopher Lengner**[6], **Fazheng Ren**[1,*], **Lixiang Xue**[2,*], and **Zhengquan Yu**[1,*]

[1]Beijing Advanced Innovation Center for Food Nutrition and Human Health and State Key Laboratories for Agrobiotechnology, College of Biological Sciences, China Agricultural University, Beijing, China

[2]Medical Research Center. Department of Radiation Oncology, Peking University Third Hospital, Beijing, China

[3]Department of Physics and State Key Laboratory of Cellular Stress Biology, Innovation Center for Cell Signaling Network, Xiamen University, Xiamen, China, 361005

[4]Department of Animal Science, Southwest University, Rongchang, Chongqing, China

[5]Department of Developmental and Cell Biology, Sue and Bill Gross Stem Cell Research, Center for Complex Biological Systems, University of California, Irvine, Irvine, California, United States of America

[6]Department of Animal Biology, School of Veterinary Medicine, and Institute for Regenerative Medicine, University of Pennsylvania, Philadelphia, Philadelphia, United States of America

Abstract

Hair follicles (HFs) undergo precisely regulated cycles of active regeneration consisting of (anagen), involution (catagen), and relative quiescence (telogen) phases. HF stem cells (HFSCs) play important roles in regenerative cycling. Elucidating mechanisms that governs HFSC behavior can help uncover the underlying principles of hair development, hair growth disorders and skin cancers. RNA-binding proteins of the Musashi (Msi) have been implicated in the biology of different stem cell types, yet they have not been studied in HFSCs. Here we utilized gain- and loss-of-function mouse models to demonstrate that forced MSI2 expression retards anagen entry and consequently, delays hair growth, while loss of *Msi2* enhances hair regrowth. Further, our findings show that *Msi2* maintains quiescent state of HFSCs in the process of telogen-to-anagen transition. At the molecular level, our unbiased transcriptome profiling shows that Msi2 represses Hh signaling activity and that *Shh* is its direct target in the HF. Taken together, our findings reveal

[*]Corresponding authors: Zhengquan Yu, Ph.D., College of Biological Sciences, China Agricultural University, No. 2 Yuanmingyuan West Road, Haidian District, Beijing, China, 100193 Tel: +86-10-62734420; FAX: +86-10-62733904; zyu@cau.edu.cn, Lixiang Xue, Ph.D., Department of Radiation Oncology, Peking University Third Hospital, No. 2 Huayuan North Road, Haidian District, Beijing, China100191; Tel: +86-13720017369; FAX: +86-10-62733904; lixiangxue@bjmu.edu.cn, Fazheng Ren, Beijing Advanced Innovation Center for Food Nutrition and Human Health, China Agricultural University, No.2 Yuanmingyuan West Road, Haidian District, Beijing, China, 100193 Tel: +86-10-62736344; FAX: +86-10-62736344; renfazheng@263.net.

[¶]These authors contributed equally to this work.

Conflict of Interest: Authors state no competing interests.

the importance of *Msi2* in suppressing hair regeneration and maintaining HFSC quiescence. Previously unreported Msi2-Shh-Gli1 pathway adds to the growing understanding of the complex network governing cyclic hair growth.

Introduction

The hair follicle (HF) undergoes recurrent regenerative cycling consisting of anagen, catagen and telogen phases (Stenn and Paus, 2001). Such cycling is sustained by the hair follicle stem cells (HFSCs), which operate under complex signaling regulation. Many signaling pathways converge to jointly regulate HFSCs, including Wnt, Bmp, Notch and Hh pathways among others (Lee and Tumbar, 2012; Millar, 2002; Plikus *et al.*, 2017; Plikus *et al.*, 2008). Elucidating the in-depth mechanisms that govern HFSC behavior is essential for understanding the principles of normal hair development and etiology of human hair growth disorders. Morphologically, HFSCs are located in the so-called follicular bulge, in close proximity to the mesenchymal dermal papilla – the principal signaling niche of the HF. Secondary hair germ (sHG) progenitors are located between HFSCs and dermal papilla, and during telogen both HFSCs and sHG progenitors remain quiescent (Cotsarelis *et al.*, 1990; Keyes *et al.*, 2013). At the onset of anagen, signals from the dermal papilla, as well as the extra-follicular macro-environment activate proliferation of sHG cells, whose progenies expand downward, envelop dermal papilla, and generate new hair matrix (Mx) (Plikus *et al.*, 2011). To sustain anagen progression, sHG-derived transit-amplifying cells (TACs) in the Mx secrete Shh that acts to activate HFSCs in the bulge (Hsu *et al.*, 2014). Throughout anagen, TACs in the Mx proliferate, move upward and terminally differentiate to form the inner root sheath (IRS) and hair shaft. To a large degree, formation of TACs represents the bottleneck in the process of hair growth cycle, and without TAC-derived Shh, quiescent HFSCs fail to activate. However, little is known about the signals that counterbalance Shh to maintain HFSC quiescence.

Musashi is an evolutionarily conserved RNA binding protein family, which was first identified in *Drosophila* (Nakamura *et al.*, 1994). In mammals, there are two orthologues: Musashi1 (MSI1/Msi1) (Sakakibara *et al.*, 1996) and MSI2/Msi2 (Sakakibara *et al.*, 2001). Msi2 has been identified as the critical regulator of tissue-specific SCs in several systems, including neural system (Sakakibara *et al.*, 2001), blood (Ito *et al.*, 2010; Kharas *et al.*, 2010; Park *et al.*, 2014; Rentas *et al.*, 2016) and intestine (Wang *et al.*, 2015). Inactivation of MSI2 in hematopoietic stem cells (HSCs) impairs their competitive repopulation ability upon transplantation (Hope *et al.*, 2010; Ito *et al.*, 2010; Kharas *et al.*, 2010). Recently, MSI2 was shown to play important roles in several types of cancers (Kang *et al.*, 2016; Katz *et al.*, 2014; Kudinov *et al.*, 2016; Wang *et al.*, 2015). Although *Msi2* was shown to be expressed in HF bulge, sHG and IRS (Sugiyama-Nakagiri *et al.*, 2006), its role in HF development and regenerative cycling remains unknown. Here we demonstrate that *Msi2* is a key post-transcriptional regulator of HFSC quiescence and that it operates by directly targeting Shh/Gli1 signaling pathway.

Results

MSI2 overexpression retards telogen to anagen transition during hair cycling

To elucidate the role of *Msi2* in hair cycling, we started by profiling its expression levels. *Msi2* is strongly expressed on day P21 during first telogen, reaches its highest levels at P36 during mid-anagen, and then decreases to its lowest levels at P42 and P49 (Figure 1a). At P21 Msi2 is primarily expressed in the bulge and sHG (Figure 1b). At P36 and P40 it is prominently expressed both in the basal and suprabasal bulge, outer root sheath (ORS), TACs and IRS (Figure 1b). At P49, when HFs enter second telogen, Msi2 becomes localized to the basal and suprabasal bulge and sHG – expression pattern that is reminiscent of that at P21. Additionally, Msi2 is expressed in the basal epidermal cells at different at different time points (Figure S1a and S1b).

Next, we generated *K14-rtTA::TRE-MSI2* double transgenic (DTG) mice in which overexpression of the conserved human MSI2 can be induced throughout the epithelial compartment of the skin (Figure S1c). Upon Dox induction, DTG mice exhibited robust *MSI2* overexpression in K14-positive skin, thymus, and esophagus, but not in K14-negative intestine (Figure S1d). The induction of MSI2 in skin was further confirmed at protein level (Figure S1e). Msi2 is specifically induced in the basal epidermal layer, ORS and follicular bulge (Figure S1f). We induced MSI2 overexpression at P21 and characterized the resulting HF phenotype. At P24, control HFs displayed early anagen morphology, while DTG HFs were still in telogen (Figure 1c). At P26, both control and DTG HFs were in anagen, albeit DTG HFs were significantly shorter (Figure S1g). When MSI2 overexpression was induced at P18, DTG phenotype became more pronounced with HFs displaying telogen morphology even at P26 (Figure 1d). Consistent with the delayed anagen entry, length of DTG HFs was shorter than in control mice (Figures 1c and 1d). Supporting this phenotype, hair regrowth after shaving is delayed in the DTG animals (Figure S1h). Together, these findings show that MSI2 overexpression significantly delays telogen-to-anagen transition and progression through anagen.

MSI2 induction impairs hair regrowth after depilation

Next, we examined the role of Msi2 during depilation-induced hair cycle. After depilation at P21, Msi2 becomes strongly expressed in sHG at P22 and in Mx at P24 (Figure S2a). We then induced MSI2 overexpression in DTG mice at P18 and depilated at P21. External hair regrowth was observed in littermate controls ten days post-depilation, but was still absent in DTG mice (Figure 2a). DTG mice eventually regrew hairs by P44 (Figure 2a). On histology, at P22 (i.e. 36 hours post-depilation) both control and DTG HFs showed extended sHG, morphological feature of anagen II (Figures 2b and S2b). At P24, control HFs elongated and featured prominent hair bulb, a feature of anagen III. At the same time, DTG HFs lacked hair bulb (Figures 2b and S2b). Normally, anagen onset is accompanied by nuclear β-Catenin, a marker of active Wnt signaling (Lo Celso *et al.*, 2004; Lowry *et al.*, 2005). Substantially fewer nuclear β-Catenin positive cells can be found in DTG HFs at P24, while no differences are seen at P22 (Figure S2c and S2d). Also, at P30 anagen DTG HFs are shorter than these in control mice (Figure 2b). Similar phenotype was observed when hairs

were depilated during second competent telogen phase (Figure S2e and S2f). These findings indicate that overexpression of MSI2 delays anagen initiation.

Next we deleted *Msi2* in the skin of *K14-Cre*::*Msi2*$^{flox/flox}$ (cKO) mice (Figure S3a). Deletion specificity in skin was confirmed by qRT-PCR (Figure S3b). Loss of Msi2 at the protein level was further confirmed by immunostaining and Western blotting (Figure S3c and S3d). Specific deletion of Msi2 was also found in the thymus, where K14 promoter is active (Figure S3e), but not in the intestine (Figure S3f). While no obvious differences were found between control and cKO HFs during natural hair cycle (Figure S3g), the downward growth of *Msi2* cKO HFs is significantly faster than in control at 72 hours post-depilation (Figures 2c and 2d). Also, length of three types of hairs in cKO mice is significantly longer than in controls 21 days after depilation (Figure S4a and S4b). Similar phenotype was also found when hairs were depilated during second competent telogen (Figure S4c and S4d). Generally, cKO phenotype is opposite of that in DTG mice. We also noticed that anagen progression in control mice for cKO is slower than in control mice for DTG (Figures 2b, 2c and S4a). This is most likely due to background strain differences. DTG mice are on FVB, while cKO mice are on mixed genetic background (C57BL/6xCBA, further crossed to Swiss Webster). For this reason, in all experiments we used littermate controls.

AE13 marks cuticle and cortex/precortex of the HF (Lynch *et al.*, 1986), while AE15 marks IRS and medulla (Me) cells (O'Guin *et al.*, 1992), and both are used as sensitive markers of HF differentiation. At P24, AE13 and AE15 positive cells are present in control, but not in DTG HFs (Figure S4e). In contrast, AE13-positive cells appear in *Msi2* cKO HFs ahead of littermate control (Figure S4e). Consistently, DTG HFs display much fewer, while cKO HFs show more proliferative cells 3 days post-depilation compared to littermate controls (Figure S4f-S4h). Importantly, no differences in the number of proliferative cells were seen between DTG, cKO and corresponding control HFs on 90 min BrdU pulse assay 24 hours post-depilation (Figure 2e). Yet, substantially fewer and more BrdU-positive cells were see in DTG and cKO HFs respectively after 48 hours pulse-tracing (Figures 2f and 2g), suggesting impaired HFSC activation in response to Msi2 induction. Together, these data shows that *MSI2* overexpression impairs, while loss of *Msi2* accelerates hair regrowth.

Msi2 maintains quiescent state of HFSCs

Previously, Msi2 is an important regulator for neural, hematopoietic and intestinal stem cells. Here, we asked if it similarly regulates HFSCs. Intriguingly, we see that the number of a6-integrin^{+}CD34^{+} HFSCs is not significantly altered in both DTG and cKO mice as compared to control (Figure S5a). Next we asked if Msi2 regulates proliferative state rather than the number of HFSCs. K15 was used to identify rapidly cycling HFSCs (Greco *et al.*, 2009; Liu *et al.*, 2003). Sox9 was used as another marker for rapidly cycling HFSCs, with expression pattern that is broader than of K15 (Vidal *et al.*, 2005). In contrast, NFATc1 was used as the marker of quiescent HFSCs, located in the upper bulge (Horsley *et al.*, 2008). Three days after induction at P21, we observed more NFATc1-positive, yet fewer K15-positive HFSCs in DTG HFs (Figure S5b). We also evaluated HFSCs in DTG and *Msi2*cKO mice 36 hours after depilation (P22), when no histological differences are discernible. For DTG HFs, we also see more NFATc1-positive and fewer K15-positive HFSCs (Figure S5c),

and decreased HFSC proliferation (Figure 3a and 3b). In contrast, cKO HFs show fewer NFATc1-positive and more K15-positive HFSCs (Figure S5d), and more proliferating HFSCs (Figures 3c and 3d). Together, these results indicate that *Msi2* functions to maintain HFSC quiescence. Previously, Lhx2 has been implicated as the regulator of HFCS quiescence (Folgueras *et al.*, 2013; Mardaryev *et al.*, 2011). Given functional similarity between Msi2 and Lhx2 activities, we examined whether the two are connected. We found fewer Lhx2-positive cells in DTG HFs three days after Dox induction at P21 (Figure S6a) or 36 hours post-depilation (Figure S6b), and more Lhx2-positive cells in cKO HFs 36 hours after depilation (Figure S6c), suggesting that Msi2 does not regulate Lhx2, and that the two likely maintain HFCS quiescence via distinct mechanisms.

Msi2 represses hair follicle neogenesis

Next, we asked whether MSI2 induction inhibits wound-induced HF neogenesis, the regenerative phenomenon that resembles embryonic HF development (Horsley *et al.*, 2008). We induced *MSI2* overexpression at P18 and wounded mice at P21. Scab detachment in DTG mice was two days delayed as compared to controls (Figure S7a). At post-wounding day (PWD) 17, HF neogenesis was largely abrogated in DTG mice (Figure S7b). Although the number of *de novo* HFs in DTG mice is much fewer than in control wounded mice at PWD 17, we noticed that more *de novo* HFs regenerated in DTG wounds by PWD 33 (Figure S7c). To further differentiate if HF neogenesis is suppressed by MSI2 rather that simply delayed, we induced MSI2 overexpression 10 days after wounding, just days ahead of HF neogenesis onset. With this induction timing, initial wound closer was not affected in DTG mice (Figure S7d). Yet, there were still significantly fewer *de novo* HFs forming in DTG mice, supporting the notion that MSI2 overexpression indeed represses HF neogenesis (Figure S7d). In contrast, more *de novo* HFs were seen to form in the wounds of *Msi2* cKO mice as compared to littermate controls at PWD 15, (Figure S7e), despite the same wound closure rates. This trend also continued at PWD 17 (Figure S7f). Taken together, these findings demonstrate that Msi2 represses wound-induced HF neogenesis.

MSI2 induction represses Shh/Gli1 signaling pathway

To gain mechanistic insights into the molecular events underlying repression of telogen-to-anagen transition by Msi2, we performed transcriptome profiling on control and DTG dorsal skin 3 days after Dox treatment (P21-P24). It reveals that *Msi2* induction drives rapid and robust changes in genes expression (Figures S8a and S8b). We identified 209 downregulated and 319 upregulated genes with a significance $q<0.05$ and a fold change >2.0 (Figure S8a). Gene ontology (GO) analysis on these 528 genes identified “keratinization” and “skin development” among the top affected biological process (Figure S8c). Surprisingly, many of the signaling pathways, including Notch, mTOR and TGFb, which had been implicated as targets of Msi2 in other organs (Okano *et al.*, 2005; Park *et al.*, 2014; Wang *et al.*, 2015), are not affected by MSI2 overexpression in skin (Figure S8d). This result was further confirmed by qRT-PCR and Western blotting (Figures S8e and S8f), and it indicates a tissue-specific mechanism for Msi2 function in the skin.

Enrichment for “basal cell carcinoma” and “Hedgehog (Hh) signaling pathway” on GO analysis (Figure S8d), known role of dysregulated Hh signaling in basal cell carcinoma

(Epstein, 2008) and established role of Hh signaling in HFSC activation (Hsu *et al.*, 2014) all point toward a potential link between Msi2 and Hh signaling pathway in HFs. Many downstream Hh target genes *Shh*, *Gli1*, *Ptch2*, *Hhip* are downregulated in DTG skin (Figure 4a). In contrast, several downstream Hh targets *Shh*, *Gli1* and *Ptch2* are upregulated in *Msi2* cKO skin (Figure 4b). Together, these data suggest that Msi2 inhibits Hh signaling.

Interestingly, the upstream gene *Shh* was downregulated in DTG mice, while upregulated in *Msi2* cKO mice both on RNA and protein levels (Figures 4a-4d). Considering that Msi2 functions as a negative regulator of gene expression via repression of protein translation (Ito *et al.*, 2010; Kharas *et al.*, 2010; Wang *et al.*, 2015) or mRNA de-stabilization (Bennett *et al.*, 2016) by directly binding to 3′UTR of target genes (Ito *et al.*, 2010; Kharas *et al.*, 2010; Okano *et al.*, 2005; Wang *et al.*, 2015), we proposed that *Shh* might be a direct target of Msi2. The binding motif of Msi2 has been identified as [5′-(G/A)U_nAGU-3′ (n=1-3)] (Imai *et al.*, 2001; Sakakibara *et al.*, 2001). After screening for Msi2 binding sites, we identified a perfectly matched motif of (5′-GUUUAGT-3′) in the conserved region of *Shh* 3′-UTR (Figure 4e). Homology analysis demonstrated the identified motif is conserved among placental mammals (Figures S9a and S9b). To further test whether 3′-UTR of *Shh* is a direct target of Msi2, we constructed luciferase reporters for the *Shh* 3′-UTRs, as well as reporter constructs in which the Msi2 binding sites were mutated. We found that wild type *Shh* 3′-UTR reporter activity was significantly repressed, but no significant change for the mutant type reporters was seen with overexpression of hMSI2 (Figure 4e). This indicates that Msi2 might directly target *Shh*. Further, CLIP-PCR assay revealed that *Shh* is enriched in the Msi2 antibody immunoprecipitates (Figure 4f), demonstrating that Msi2 physically binds to 3′UTR of *Shh* mRNA. Thbs1, a known Msi2 target in skin, was used as the positive control (Bennett *et al.*, 2016). Interestingly, *Numb* and *Pten*, which have been identified as Msi2 targets in intestine (Wang *et al.*, 2015), were not enriched in the Msi2 antibody immunoprecipitates of skin keratinocytes (Figure 4f). This data suggests that Msi2 has unique targets in different organs. *In situ* hybridization further revealed that Msi2 and *Shh* co-localize in the Mx and activated sHG of HFs (Figure 4g, S10a and S10b), implying direct interaction between Msi2 and *Shh* in the process of HF development. Further, we reveal that Msi2 induction promotes decays of *Shh* mRNA (Figure 4h). Consistently, *Shh* mRNA is reduced in DTG HFs at 36 hours and 3 days post-depilation, and upregulated in Msi2 cKO HFs (Figure S10a and S10b). Together, these findings demonstrate that Msi2 represses gene expression of Shh by de-stabilizing *Shh* mRNA.

Next, we asked whether *Shh* repression mediated by Msi2 functionally regulates hair regrowth following depilation. *Shh* is induced starting 24 hours post-depilation when sHG enlarges and TACs form (Hsu *et al.*, 2014). Thus, we examined expression of *Shh* in DTG and cKO HFs 36 hours post-depilation. We observe prominent reduction of *Shh* in DTG mice and moderate increase in cKO mice at the mRNA and protein levels (Figures 5a-5c). Gli1 is a readout target of Shh signaling. We found that Gli1 is highly expressed in the TACs of Mx in control, but not DTG HFs (Figures 5a, 5c and S10c). In contrast, Gli1 is increased in the Mx of cKO HFs (Figures 5b, 5c and S10c). Cyclin D1 is another known downstream target of Shh (Hsu *et al.*, 2014; Kenney and Rowitch, 2000). In agreement, Cyclin D1 is reduced in sHG of DTG and increased in sHG of cKO regenerated HFs (Figures 5c and 5d). Shh signaling also downregulates BMP-specific p-Smad1/5/8, which is required for early

anagen progression (Kenney and Rowitch, 2000). Consistently, p-Smad1/5/8 is upregulated in DTG and downregulated in cKO HFs (Figures 5c and 5e). Considering that Msi1 is another mammalian ortholog of Msi2 and it functions redundantly in some tissues (Sakakibara *et al.*, 2001; Wang *et al.*, 2015), we tested Msi1 expression. We show that it is not altered in both DTG and cKO mice (Figure 5c). To further confirm this model, we performed rescue experiment with Hh agonist, SAG (Heine *et al.*, 2011; Paladini *et al.*, 2005). Western blotting for Gli1 confirmed that SAG activated Hh signaling (Figure S10d). In comparison to control mice, vehicle-treated dorsal skin of DTG mice exhibited delayed external hair regrowth and delayed anagen progression (Figure 5f). However, SAG treated dorsal skin showed faster hair regrowth in DTG mice (Figure 5f). These findings suggest that activation of Hh signaling pathway is able to rescue hair cycle inhibition caused by MSI2 overexpression (Figure 5f). Together, our findings show that Msi2 represses Hh pathway activity to regulate hair regrowth after depilation.

In summary, our findings reveal the importance of Msi2 in suppressing hair regeneration and maintaining HFSC quiescence during telogen-to-anagen transition. We provide in vivo evidence for a previously unreported mechanism of Shh-Gli1 pathway repression by Msi2 (Figure 5g), adding to the growing understanding of the complex signaling network that governs cyclic hair growth.

Discussion

Transient activation of quiescent HFSCs is necessary for sustained cyclic activation of HF regrowth (Rompolas and Greco, 2014). Signaling network that drives their activation consists of multiple pathways, including but not limited to Shh and Wnt (Rompolas and Greco, 2014). Particularly, Shh has recently been identified as an important signal that emanates from TACs during early anagen and drives proliferative activation of the adjacent bulge HFSCs (Hsu *et al.*, 2014). Here we found that *Msi2* maintains quiescent state of HFSCs by directly targeting Shh. Interestingly, Msi2 expression levels are elevated during physiological anagen and in response to hair cycle activation by depilation, states when HFSCs undergo activation. Thus, our findings suggest that rather than locking HFSCs in prolonged quiescence during telogen, Msi2 fine-tunes HFSCs activation by Shh during anagen initiation.

Previous studies implicated Msi2 as a critical regulator of murine hematopoietic and intestinal stem cell self-renewal and fate determination (Ito *et al.*, 2010; Kharas *et al.*, 2010; Park *et al.*, 2014; Wang *et al.*, 2015). Msi2 is a general regulator of somatic SCs in a variety of organs. Importantly, in contrast to its role in promoting SC quiescence in the HF, Msi2 promotes proliferation of HSCs and ISCs in the bone marrow and intestine respectively (Ito *et al.*, 2010; Kharas *et al.*, 2010; Park *et al.*, 2014; Wang *et al.*, 2015). This indicates that specific Msi2 functions in tissue- and SC type-dependent. Opposing roles for Msi2 were shown in the context of cancer. Msi2 has been identified as a tumor suppressor in breast cancer, where it represses epithelial-to-mesenchymal transition (Katz *et al.*, 2014). However, in colorectal cancer and leukemia it functions as an oncoprotein (Ito *et al.*, 2010; Kharas *et al.*, 2010; Park *et al.*, 2014; Wang *et al.*, 2015).

Mechanistically, we show that Msi2 promotes HFSC quiescence by directly repressing *Shh*. MSI2 overexpressing HFs display reduced proliferation in the bulge and hair bulb, resembling phenotype of Shh-cKO mice (Hsu *et al.*, 2014). In contrast, increased HFSC proliferation is seen in *Msi2* cKO HFs after depilation. TAC pool would wane if they cannot produce Shh, which could explain the delayed grows of HFs in MSI2 overexpressing mice following depilation. Based on our data we propose a model where restriction of Shh signaling by Msi2 fine-tunes the process of quiescent HFSC activation (Figure 5g). We noticed that the Hh downstream target Ptch1 is not significantly altered in both DTG and cKO mice. This suggests that the regulation of Hh downstream targets is complex, and likely context dependent. Overactive Hedgehog (Hh) signaling is essential for basal cell carcinoma development (Epstein, 2008; Kasper *et al.*, 2012), and overexpression of Shh, Gli1 and/or Smo induced basal cell carcinomas in mice (Dahmane *et al.*, 1997; Oro *et al.*, 1997). We speculate that Msi2 can act as the potential inhibitor of basal cell carcinomas – a possibility that can be examined in the future studies.

Previous works identified several targets for Msi2, including Numb, Pten, and TGFb. *Msi2* repress translation of *Numb* in neural precursors (Okano *et al.*, 2005) and in malignant hematopoietic cells (Ito *et al.*, 2010; Kharas *et al.*, 2010). Msi2 governs HSC self-renewal and cell fate determination by modulating cells' sensitivity to TGFβ signaling (Park *et al.*, 2014). It also drives intestinal transformation by targeting tumor suppressor, *Pten* (Wang *et al.*,2015). However, the above targets are not altered in skin of MSI2 overexpressing mice and *Msi2* cKO mice, further highlighting tissue specificity of Msi2 mechanism of action. In summary, we reveal that Msi2 plays an important role in maintaining quiescent state of HFSCs via Msi2-Shh-Gli1 signaling axis during HF regeneration.

Materials and Methods

Detailed materials and methods in the Supplementary Materials

All animal procedures were evaluated and authorized by the Beijing Laboratory Animal Management. All animal studies were performed in strict adherence to the Institutional Animal Care and Use Committee (IACUC) guidelines of China Agricultural University (approval number: SKLAB-2011-04-03).

Wounding and whole-mount hair follicle neogenesis assay

Wound-induced hair neogenesis assay was performed as previously described (Horsley *et al.*, 2008; Yuan *et al.*, 2015). Full-thickness 2.25 cm^2 wounds were created on dorsal skin at P21 in mice anaesthetized with sodium pentobarbital. For *de novo* HF analysis, mice were sacrificed at 15 or 17 days post-wounding.

Dual luciferase activity assay

Shh 3′UTR fragment containing binding site (5′-GUUUAGT-3′) was cloned into the psiCHECK-2 vector (Promega, Madison, WI). The mutant binding site was 5′-GGGTTCG-3′, obtained by a QuikChange Site-Directed Mutagenesis kit (Stratagene, St Clara, CA). 10 ng of *Shh* and mutant reporter constructs were co-transfected with human MSI2 overexpressing vector (hMSI2) or a negative control (his) into 293T cells,

respectively. The activity of Firefly and Renilla luciferase were measured with the Dual-Glo luciferase assay system (Promega, Madison, WI). The primers was: forward: 5′-AAAGCGCACGGAAGGAG-3′; reverse: 5′- CGCAGGACAAGGGACAT-3′.

CLIP-qPCR

CLIP-qPCR assay performed as previously described with modification (Wang *et al.*,2015). Briefly, cell suspensions of lower HF were irradiated twice at 400 mJ/cm^2, and then lysed using PXL buffer. After spinning, the supernatant was added to protein A Dynabeads (Dynal, 100.02, Thermo Fisher, Fremont, CA), conjugated with anti-Msi2 antibody (Abcam, Cambridge, United Kingdom) or goat anti-rabbit IgG (Jackson ImmunoResearch, West Grove, PA) and incubated for 4 hours at 4°C. Beads were washed and digested with Proteinase K. RNA was extracted from beads and then quantified with qRT-PCR.

RNA stability measurements

The RNA decays curve assay were performed as previously described (Bennett *et al.*, 2016). Briefly, Lovo cells were transfected with 1 mg human MSI2 overexpressing vector (hMSI2) or a negative control (his). RNA was measured at 0, 2, 4, 6 and 8 h using qRT-PCR.

Supplementary Material

Refer to Web version on PubMed Central for supplementary material.

Acknowledgments

ZY is supported by the Major Project for Cultivation Technology (2016ZX0800800120l4ZX08008001); NSFC (No.81572614, 31271584); Beijing Nature Foundation Grant (5162018); Basic Research Program (2015QC0104, 2015TC041, 2016SY001, 2016QC086); SKLB Open Grant (2015SKLB6-16). LX is supported by the NSFC (No. 81541142, 81672091). MVP is supported by the NIH NIAMS grants R01-AR067273, R01-AR069653. We thank Shukai Yuan, Feifei Li, Liang Zhong for the kindly helps in sharing methods and in submitting the RNA-Seq data and thank Liying Du in the Core Facilities at School of Life Sciences, Peking University for sorting the HFSCs.

References

Bennett CG, Riemondy K, Chapnick DA, Bunker E, Liu X, Kuersten S, et al. Genome-wide analysis of Musashi-2 targets reveals novel functions in governing epithelial cell migration. Nucleic Acids Res. 2016; 44:3788–800. [PubMed: 27034466]

Cotsarelis G, Sun TT, Lavker RM. Label-retaining cells reside in the bulge area of pilosebaceous unit: implications for follicular stem cells, hair cycle, and skin carcinogenesis. Cell. 1990; 61:1329–37. [PubMed: 2364430]

Dahmane N, Lee J, Robins P, Heller P, Ruiz i Altaba A. Activation of the transcription factor Gli1 and the Sonic hedgehog signalling pathway in skin tumours. Nature. 1997; 389:876–81. [PubMed: 9349822]

Epstein EH. Basal cell carcinomas: attack of the hedgehog. Nat Rev Cancer. 2008; 8:743–54. [PubMed: 18813320]

Folgueras AR, Guo X, Pasolli HA, Stokes N, Polak L, Zheng D, et al. Architectural niche organization by LHX2 is linked to hair follicle stem cell function. Cell Stem Cell. 2013; 13:314–27. [PubMed: 24012369]

Greco V, Chen T, Rendl M, Schober M, Pasolli HA, Stokes N, et al. A two-step mechanism for stem cell activation during hair regeneration. Cell Stem Cell. 2009; 4:155–69. [PubMed: 19200804]

Heine VM, Griveau A, Chapin C, Ballard PL, Chen JK, Rowitch DH. A small-molecule smoothened agonist prevents glucocorticoid-induced neonatal cerebellar injury. Sci Transl Med. 2011; 3:105ra4.

Hope KJ, Cellot S, Ting SB, MacRae T, Mayotte N, Iscove NN, et al. An RNAi screen identifies Msi2 and Prox1 as having opposite roles in the regulation of hematopoietic stem cell activity. Cell Stem Cell. 2010; 7:101–13. [PubMed: 20621054]

Horsley V, Aliprantis AO, Polak L, Glimcher LH, Fuchs E. NFATc1 balances quiescence and proliferation of skin stem cells. Cell. 2008; 132:299–310. [PubMed: 18243104]

Hsu YC, Li L, Fuchs E. Transit-amplifying cells orchestrate stem cell activity and tissue regeneration. Cell. 2014; 157:935–49. [PubMed: 24813615]

Imai T, Tokunaga A, Yoshida T, Hashimoto M, Mikoshiba K, Weinmaster G, et al. The neural RNA-binding protein Musashi1 translationally regulates mammalian numb gene expression by interacting with its mRNA. Mol Cell Biol. 2001; 21:3888–900. [PubMed: 11359897]

Ito T, Kwon HY, Zimdahl B, Congdon KL, Blum J, Lento WE, et al. Regulation of myeloid leukaemia by the cell-fate determinant Musashi. Nature. 2010; 466:765–8. [PubMed: 20639863]

Kang MH, Jeong KJ, Kim WY, Lee HJ, Gong G, Suh N, et al. Musashi RNA-binding protein 2 regulates estrogen receptor 1 function in breast cancer. Oncogene. 2016

Kasper M, Jaks V, Hohl D, Toftgard R. Basal cell carcinoma - molecular biology and potential new therapies. J Clin Invest. 2012; 122:455–63. [PubMed: 22293184]

Katz Y, Li F, Lambert NJ, Sokol ES, Tam WL, Cheng AW, et al. Musashi proteins are post-transcriptional regulators of the epithelial-luminal cell state. Elife. 2014; 3:e03915. [PubMed: 25380226]

Kenney AM, Rowitch DH. Sonic hedgehog promotes G(1) cyclin expression and sustained cell cycle progression in mammalian neuronal precursors. Mol Cell Biol. 2000; 20:9055–67. [PubMed: 11074003]

Keyes BE, Segal JP, Heller E, Lien WH, Chang CY, Guo X, et al. Nfatc1 orchestrates aging in hair follicle stem cells. Proc Natl Acad Sci U S A. 2013; 110:E4950–9. [PubMed: 24282298]

Kharas MG, Lengner CJ, Al-Shahrour F, Bullinger L, Ball B, Zaidi S, et al. Musashi-2 regulates normal hematopoiesis and promotes aggressive myeloid leukemia. Nat Med. 2010; 16:903–8. [PubMed: 20616797]

Kudinov AE, Deneka A, Nikonova AS, Beck TN, Ahn YH, Liu X, et al. Musashi-2 (MSI2) supports TGF-beta signaling and inhibits claudins to promote non-small cell lung cancer (NSCLC) metastasis. Proc Natl Acad Sci U S A. 2016; 113:6955–60. [PubMed: 27274057]

Lee J, Tumbar T. Hairy tale of signaling in hair follicle development and cycling. Semin Cell Dev Biol. 2012; 23:906–16. [PubMed: 22939761]

Liu Y, Lyle S, Yang Z, Cotsarelis G. Keratin 15 promoter targets putative epithelial stem cells in the hair follicle bulge. J Invest Dermatol. 2003; 121:963–8. [PubMed: 14708593]

Lo Celso C, Prowse DM, Watt FM. Transient activation of beta-catenin signalling in adult mouse epidermis is sufficient to induce new hair follicles but continuous activation is required to maintain hair follicle tumours. Development. 2004; 131:1787–99. [PubMed: 15084463]

Lowry WE, Blanpain C, Nowak JA, Guasch G, Lewis L, Fuchs E. Defining the impact of beta-catenin/Tcf transactivation on epithelial stem cells. Genes Dev. 2005; 19:1596–611. [PubMed: 15961525]

Lynch MH, O'Guin WM, Hardy C, Mak L, Sun TT. Acidic and basic hair/nail (“hard”) keratins: their colocalization in upper cortical and cuticle cells of the human hair follicle and their relationship to “soft” keratins. J Cell Biol. 1986; 103:2593–606. [PubMed: 2432071]

Mardaryev AN, Meier N, Poterlowicz K, Sharov AA, Sharova TY, Ahmed MI, et al. Lhx2 differentially regulates Sox9, Tcf4 and Lgr5 in hair follicle stem cells to promote epidermal regeneration after injury. Development. 2011; 138:4843–52. [PubMed: 22028024]

Millar SE. Molecular mechanisms regulating hair follicle development. J Invest Dermatol. 2002; 118:216–25. [PubMed: 11841536]

Nakamura M, Okano H, Blendy JA, Montell C. Musashi, a neural RNA-binding protein required for Drosophila adult external sensory organ development. Neuron. 1994; 13:67–81. [PubMed: 8043282]

O'Guin WM, Sun TT, Manabe M. Interaction of trichohyalin with intermediate filaments: three immunologically defined stages of trichohyalin maturation. J Invest Dermatol. 1992; 98:24–32. [PubMed: 1728637]

Okano H, Kawahara H, Toriya M, Nakao K, Shibata S, Imai T. Function of RNA-binding protein Musashi-1 in stem cells. Exp Cell Res. 2005; 306:349–56. [PubMed: 15925591]

Oro AE, Higgins KM, Hu Z, Bonifas JM, Epstein EH Jr, Scott MP. Basal cell carcinomas in mice overexpressing sonic hedgehog. Science. 1997; 276:817–21. [PubMed: 9115210]

Paladini RD, Saleh J, Qian C, Xu GX, Rubin LL. Modulation of hair growth with small molecule agonists of the hedgehog signaling pathway. J Invest Dermatol. 2005; 125:638–46. [PubMed: 16185261]

Park SM, Deering RP, Lu Y, Tivnan P, Lianoglou S, Al-Shahrour F, et al. Musashi-2 controls cell fate, lineage bias, and TGF-beta signaling in HSCs. J Exp Med. 2014; 211:71–87. [PubMed: 24395885]

Plikus MV, Baker RE, Chen CC, Fare C, de la Cruz D, Andl T, et al. Self-organizing and stochastic behaviors during the regeneration of hair stem cells. Science. 2011; 332:586–9. [PubMed: 21527712]

Plikus MV, Guerrero-Juarez CF, Ito M, Li YR, Dedhia PH, Zheng Y, et al. Regeneration of fat cells from myofibroblasts during wound healing. Science. 2017

Plikus MV, Mayer JA, de la Cruz D, Baker RE, Maini PK, Maxson R, et al. Cyclic dermal BMP signalling regulates stem cell activation during hair regeneration. Nature. 2008; 451:340–4. [PubMed: 18202659]

Rentas S, Holzapfel NT, Belew MS, Pratt GA, Voisin V, Wilhelm BT, et al. Musashi-2 attenuates AHR signalling to expand human haematopoietic stem cells. Nature. 2016; 532:508–11. [PubMed: 27121842]

Rompolas P, Greco V. Stem cell dynamics in the hair follicle niche. Semin Cell Dev Biol. 2014; 25-26:34–42. [PubMed: 24361866]

Sakakibara S, Imai T, Hamaguchi K, Okabe M, Aruga J, Nakajima K, et al. Mouse-Musashi-1, a neural RNA-binding protein highly enriched in the mammalian CNS stem cell. Dev Biol. 1996; 176:230–42. [PubMed: 8660864]

Sakakibara S, Nakamura Y, Satoh H, Okano H. Rna-binding protein Musashi2: developmentally regulated expression in neural precursor cells and subpopulations of neurons in mammalian CNS. J Neurosci. 2001; 21:8091–107. [PubMed: 11588182]

Stenn KS, Paus R. Controls of hair follicle cycling. Physiol Rev. 2001; 81:449–94. [PubMed: 11152763]

Sugiyama-Nakagiri Y, Akiyama M, Shibata S, Okano H, Shimizu H. Expression of RNA-binding protein Musashi in hair follicle development and hair cycle progression. Am J Pathol. 2006; 168:80–92. [PubMed: 16400011]

Vidal VP, Chaboissier MC, Lutzkendorf S, Cotsarelis G, Mill P, Hui CC, et al. Sox9 is essential for outer root sheath differentiation and the formation of the hair stem cell compartment. Curr Biol. 2005; 15:1340–51. [PubMed: 16085486]

Wang S, Li N, Yousefi M, Nakauka-Ddamba A, Li F, Parada K, et al. Transformation of the intestinal epithelium by the MSI2 RNA-binding protein. Nat Commun. 2015; 6:6517. [PubMed: 25774828]

Yuan S, Li F, Meng Q, Zhao Y, Chen L, Zhang H, et al. Post-transcriptional Regulation of Keratinocyte Progenitor Cell Expansion, Differentiation and Hair Follicle Regression by miR-22. PLoS Genet. 2015; 11:e1005253. [PubMed: 26020521]

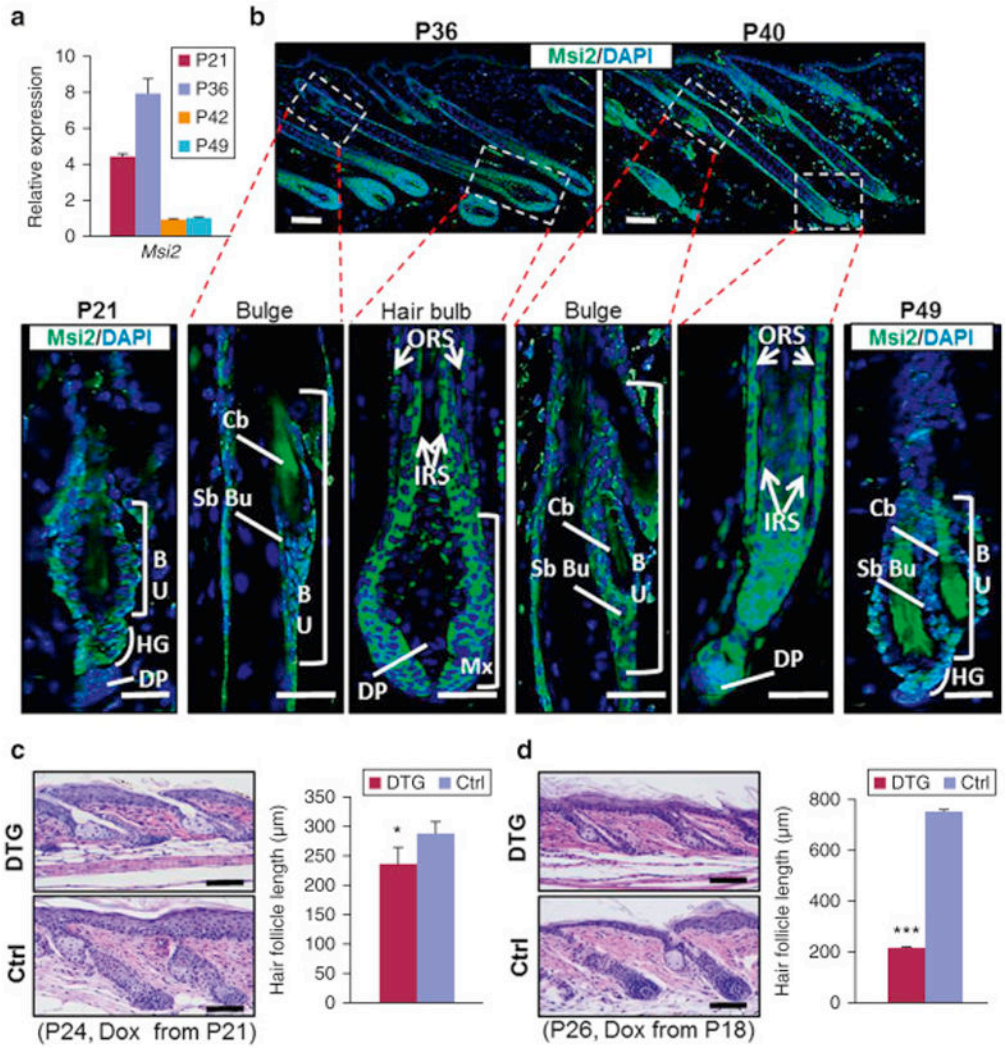

Figure 1. Forced MSI2 expression retards telogen-to-anagen transition

(**a**) qRT-PCR for *Msi2* in WT mouse skin at indicated time points. (**b**) Immunostaining for Msi2 in WT HFs at indicated time points. Arrows point to Msi2 positive signals. Dashed boxes outline magnified regions. (**c, d**) Representative histological images of dorsal skin from control (Ctrl) and DTG mice under indicated conditions. Quantification of HF length in gender-matched littermates between control (n=3) and DTG mice (n=3) at P24 (**c**) and P26 (**d**). n 3 3 biological replicates. * $p<0.05$; *** $p<0.001$. Scale bars: 50 mm.

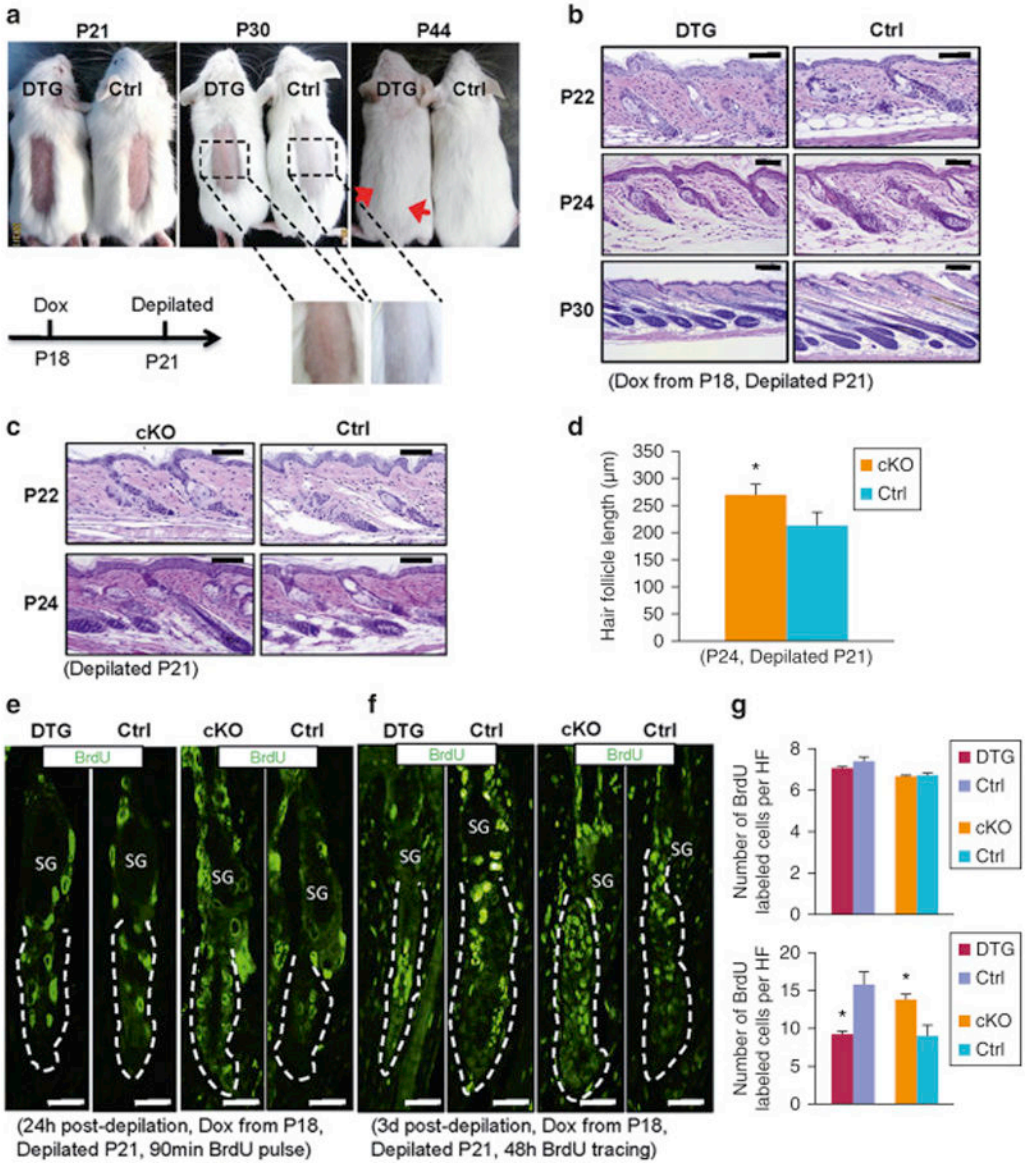

Figure 2. MSI2 induction impairs hair regrowth after depilation

(**a**) Gross images of depilated Dox-treated (from P18) control (n=5) and DTG mice (n=4) at indicated time points. Red arrows mark depilation boundaries. (**b, c**) Histology of dorsal skin from control and DTG (**b**), and control and cKO mice (**c**) at indicated time points after depilation. (**d**) Statistics of HF length in control (n=3) and cKO mice (n=3) at P24. (**e, f**) Immunofluorescence for BrdU in control and DTG, or control and cKO HFs at indicated conditions after 90 min (**e**) and 48 hours (**f**) of BrdU pulse. Dashed lines mark HFs. n = 3. (**g**) Quantification of BrdU labeled cells per HF (BU+sHGs) for (**e,** top) and (**f,** bottom). * $p<0.05$. Scale bars: 50 mm.

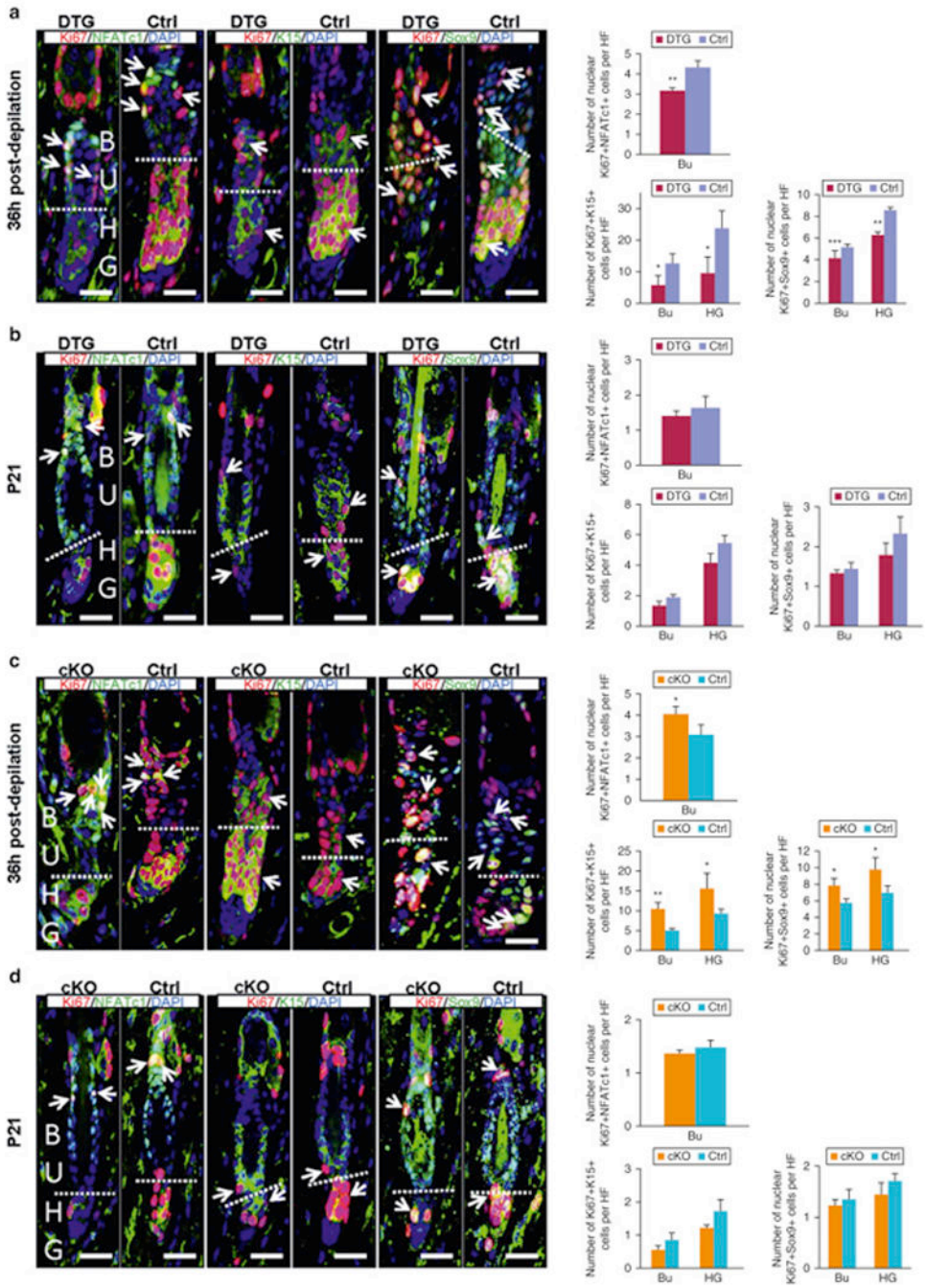

Figure 3. Msi2 maintains quiescent state of HFSCs

(**a, b**) Co-immunofluorescence for NFATc1/Ki67, K15/Ki67 and Sox9/Ki67 in control and DTG HF under conditions of 36 hours post-depilation at P21 (**a**), and pre-depilation at P21 (**b**), Pretreated with Dox at P18**;** (**c**, **d**) Co-immunofluorescence for NFATc1/Ki67, K15/Ki67 and Sox9/Ki67 in control and cKO HFs 36 hours post-depilation at P21 (**c**) and pre-depilation at P21 (**d**). The dashed line: boundary of BU and HG. Arrows: the double positive signal. (**a-d**) Quantification of $NFATc1^{+}Ki67^{+}$, $K15^{+}/Ki67^{+}$ and $Sox9^{+}Ki67^{+}$ cells in the corresponding conditions. n = 3. * $p<0.05$; ** $p<0.01$;*** $p<0.001$. Scale bar, 50 mm.

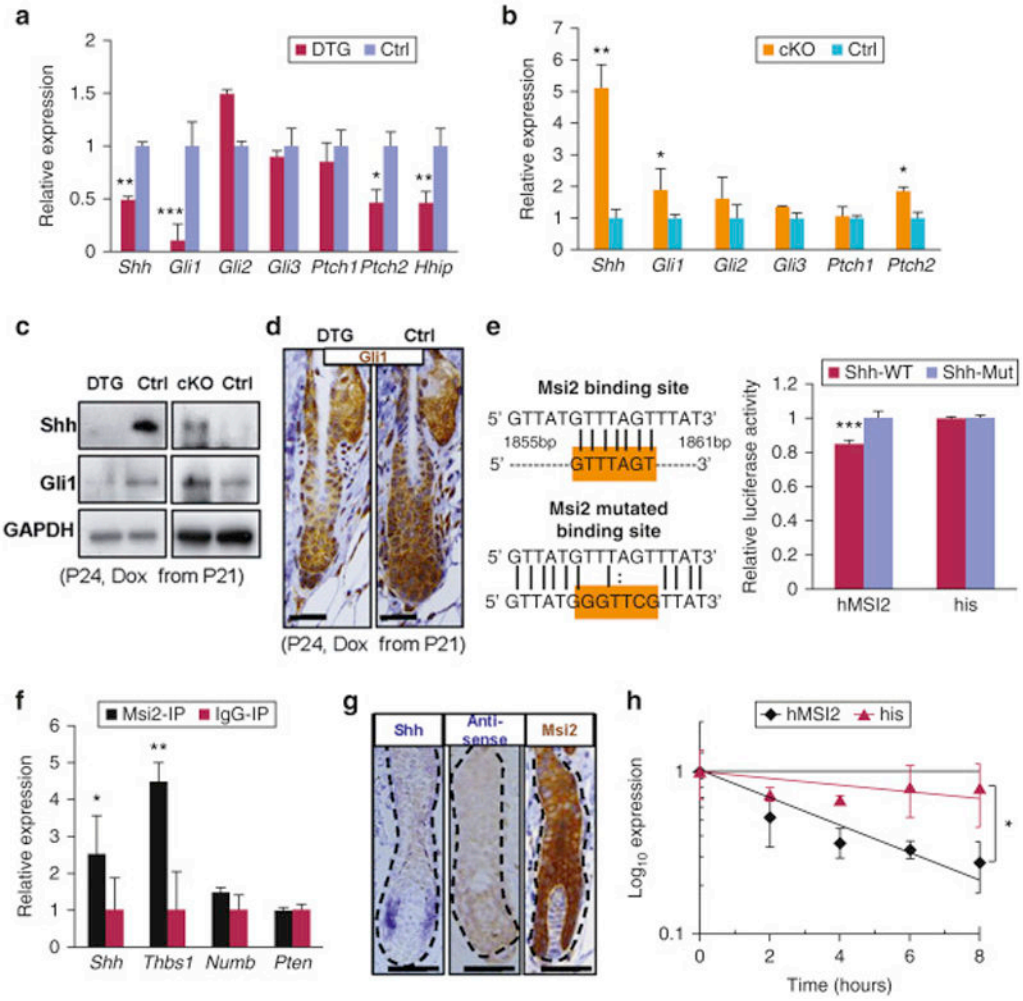

Figure 4. Msi2 directly targets Shh

(**a, b**) qRT-PCR for *Shh* and the Hh downstream genes DTG mice following Dox treatment (P21-P24) (**a**), and in cKO mice at P24 (**b**). (**c**) Western blotting for Shh and Gli1 in DTG and cKO skin at P24. (**d**) Immunostaining for Gli1 in DTG follicles at P24. Scale bar, 50 mm. (**e**) The WT and mutant binding sites of *Msi2* in 3′UTR of *Shh*. Luciferase reporter activity of *Msi2* WT and mutant 3′UTR constructs. His: vector without *MSI2*. (**f**) CLIP-PCR assay for Shh, Thbs1, Numb upon Msi2 antibody immunoprecipitates. (**g**) *In-Situ* hybridization for Shh and IHC for Msi2 in WT HFs at P24. (**h**) Shh RNA decays curve upon human MSI2 overexpression treatment. n = 3. * p<0.05, ** p<0.01, *** p<0.001.

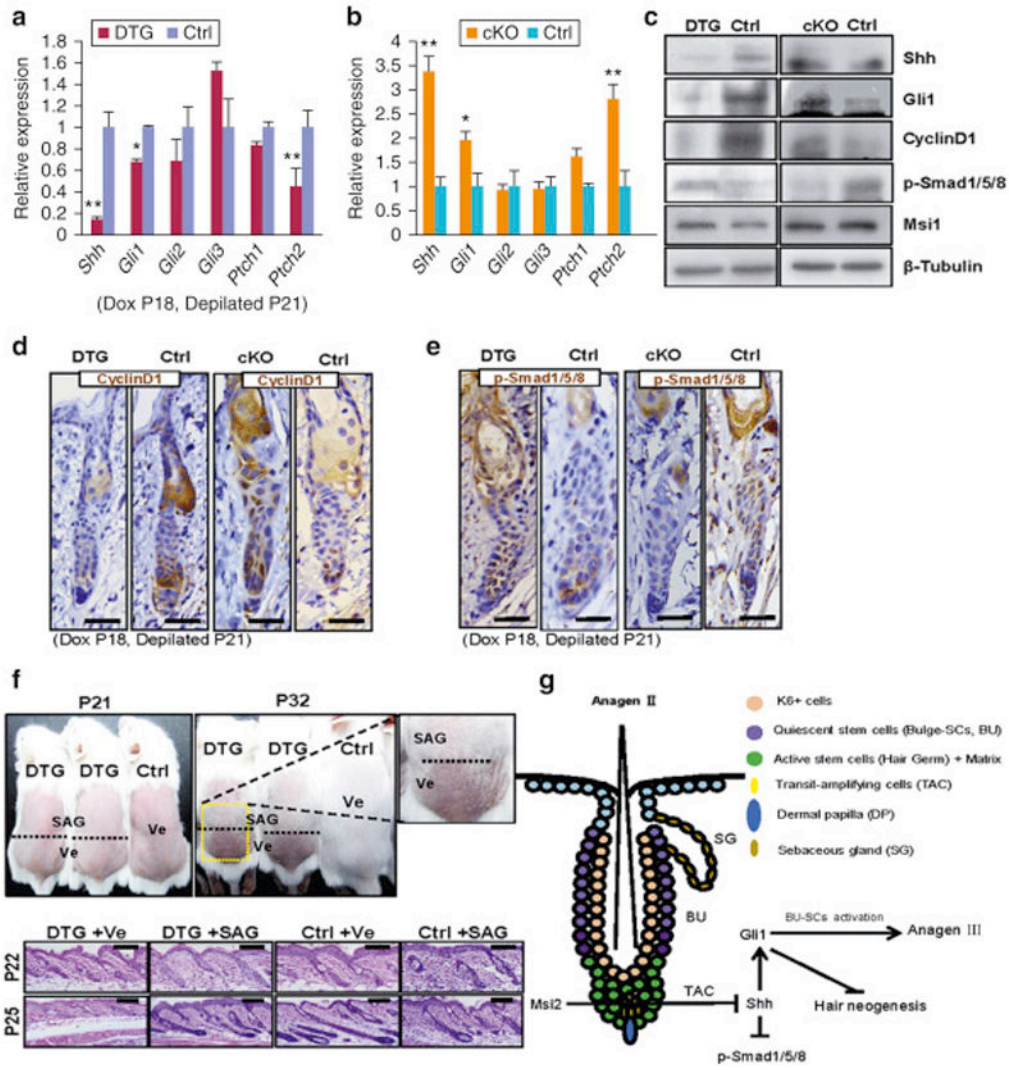

Figure 5. Msi2 represses Hh signaling after depilation

(**a, b**) qRT-PCR for *Shh* and Hh downstream genes in DTG mice (**a**), and cKO mice (**b**) 36 hours post-depilation at P21. (**c-e**) Western blotting for Shh, Gli1, Cyclin D1, p-Smad1/5/8, Msi1 (**c**), and IHC for Cyclin D1 (**d**) and p-Smad1/5/8 (**e**) in DTG and cKO skin 36 hours post-depilation at P21. (**f**) Administration of SAG rescues the delayed hair regrowth after depilation at P21. The dashed line: boundary of SAG (Upper) and Ve (Lower) treatment. Histology of skin from control and DTG mice under indicated conditions at P22 (36h post-depilation) and P25. (DTG, n=4; Control, n=7). Scale bar, 50 mm. (**g**) Schematic of *Msi2* working model in HFSCs. n = 3. * $p<0.05$, ** $p<0.01$.